particles

Article

Shell Structure Evolution of U, Pu, and Cm Isotopes with Deformed Relativistic Hartree–Bogoliubov Theory in a Continuum

Liang Wu [1], Wei Zhang [1,*], Jing Peng [2,*] and Jinke Huang [1,3]

1 School of Physics, Zhengzhou University, Zhengzhou 450001, China
2 Department of Physics, Beijing Normal University, Beijing 100875, China
3 Haimen Experimental School, Nantong 226199, China
* Correspondence: zw76@pku.org.cn (W.Z.); jpeng@bnu.edu.cn (J.P.)

Abstract: By adopting the deformed relativistic Hartree–Bogoliubov theory in continuum (DRHBc) with the point-coupling density functional PC-PK1, we investigate the shell structure evolution of even–even U, Pu, and Cm isotopic chains from the proton drip line to the neutron drip line. The Fermi energy λ_n, two-neutron separation energy S_{2n}, two-neutron shell gap δ_{2n}, and quadrupole deformation β_2 all indicate the major shell closures at N = 126, 184, and 258. The emergence of sudden drops between U and Pu isotopic chains in the proton Fermi energies λ_p around these neutron shell closures is a consequence of the designation convention when the pairing collapse at the spurious shell closure Z = 92 occurs. The fine structure in the two-neutron shell gap, like negative δ_{2n}, may be related to the ground-state shape transition. Finally, the subshells indicated by the small-scale peaks in the two-neutron shell gaps can be well understood by the deformed gaps in the single-neutron levels obtained by DRHBc theory.

Keywords: DRHBc; shell structure; neutron drip line; single-particle levels; deformed shell

check for updates

Academic Editor: Armen Sedrakian

Received: 24 December 2024
Revised: 23 January 2025
Accepted: 27 January 2025
Published: 14 February 2025

Citation: Wu, L.; Zhang, W.; Peng, J.; Huang, J. Shell Structure Evolution of U, Pu, and Cm Isotopes with Deformed Relativistic Hartree–Bogoliubov Theory in a Continuum. *Particles* **2025**, *8*, 19. https://doi.org/10.3390/particles8010019

1. Introduction

The shell structure evolution of nuclei has been extensively studied in many efforts, playing an important role in nuclear physics and astrophysics [1,2]. Currently, many nuclear experimental facilities aiming at the exploration of exotic nuclei away from the β-stability valley are in use or under construction, such as the High-Intensity Heavy Ion Accelerator Facility (HIAF) in China [3], the Radioactive Ion Beam Factory (RIBF) in Japan [4], and the Facility for Rare Isotope Beams (FRIB) in the United States [5]. Over the years, experiments have led to a series of discoveries concerning the occurrence of new magic numbers and the disappearance of traditional magic numbers, for instance, evidence for shell closures at $N = 32$, 34 in ^{54}Ti [6] and ^{54}Ga [7], and the local $N = 40$ shell closure in the magic Ni isotopic chain [8].

Theoretically, the density functional theory provides a microscopic and self-consistent way to globally study the structure of atomic nuclei across the nuclear landscape [9,10]. For non-relativistic approaches, the calculation mass table has been conducted using Skyrme [11–14] or Gogny [15–17] Hartree–Fock–Bogoliubov density functional theories. For relativistic approaches, covariant density functional theory (CDFT) can provide a self-consistent description and has made significant advances as well [10,18–24].

Based on CDFT, considering pairing correlations, continuum effects, and axial deformation degrees of freedom simultaneously, the deformed relativistic Hartree–Bogoliubov theory in continuum (DRHBc) was developed [25,26]. Currently, DRHBc theory, grounded on the point-coupling density functional PC-PK1 [27], has evolved strategies and technologies for even-Z nuclei [28,29]. It has recently been applied to construct mass tables for even-Z nuclei in Refs. [30,31], and mass tables for odd-Z nuclei are currently in development. Many interesting topics have been discussed along this line. Specifically, DRHBc theory has been used to study the ground state properties of $Z = 6$ isotopic chains, with a particular focus on the study of the neutron halo phenomenon [32]. In addition, DRHBc theory has been applied to the research of the neutron drip line nuclei of superheavy nuclear regions with Z = 106, 108, 110; even–even neutron-rich regions with Z = 8 to Z = 20; and the position of neutron drip line nuclei for isotopic chains with Z = 50 to Z = 70 [33–35]. Moreover, DRHBc theory has successfully described the odd–even staggering and the kink structure in the charge radii of mercury isotopic chains [36]. It is worth noting that DRHBc theory has also been used to explore changes in quadrupole deformation with neutron number in Te, Xe, and Ba isotopic chains, and an interesting phenomenon is that as the neutron increases, all these isotopic chains exhibit a common characteristic of prolate-shape dominance [37]. Additionally, DRHBc theory has been used for a systematic study of shell structures. It not only successfully reproduces experimental data [38] and verifies the magic numbers but also reproduces the disappearance of traditional magic numbers and the emergence of new magic numbers [39]. The inner fission barriers of even–even uranium isotopes are studied studies using DRHBc theory, and a periodic-like behavior is exhibited: peaks at the shell closures and valleys in the mid-shells [40]. These research achievements fully demonstrate the wide applicability and accuracy of DRHBc theory in nuclear physics and astrophysics research.

In this paper, we will focus on the shell structure evolution in the even–even U, Pu, and Cm isotopic chains by adopting DRHBc theory. It is interesting to note that in a very recent experimental work [41], the proton drip line of their odd-Z neighboring element Np has been determined to be ^{219}Np, which marks the heaviest proton drip line ever reached. The established α-decay systematics suggested the robustness of the $N = 126$ shell closure even in the vicinity of the proton drip line [41]. Besides, it is fascinating to explore the possible shell closures, subshell structures, and their evolution in the neutron-rich region.

2. Theoretical Framework

The details of DRHBc theory can be found in Refs. [26,28,30,42]. Here, we only briefly introduce its formalism. In DRHBc theory, the relativistic Hartree–Bogoliubov (RHB) equation that self-consistently describes mean field potentials and pairing correlations reads

$$\begin{pmatrix} \hat{h}_D - \lambda_\tau & \hat{\Delta} \\ -\hat{\Delta}^* & -\hat{h}_D^* + \lambda_\tau \end{pmatrix} \begin{pmatrix} U_k \\ V_k \end{pmatrix} = E_k \begin{pmatrix} U_k \\ V_k \end{pmatrix}, \tag{1}$$

where $\hat{h}_D$ is the Dirac Hamiltonian, λ_τ $(\tau = n, p)$ is the Fermi energy for neutron or proton, $\hat{\Delta}$ is the pairing potential, U_k and V_k are the quasiparticle wave functions, and E_k is the quasiparticle energy. In the coordinate space, the Dirac Hamiltonian is

$$h_D(\boldsymbol{r}) = \boldsymbol{\alpha} \cdot \boldsymbol{p} + V(\boldsymbol{r}) + \beta[M + S(\boldsymbol{r})], \tag{2}$$

where M is the nucleon mass, $S(\boldsymbol{r})$ and $V(\boldsymbol{r})$ are the scalar and vector potentials. The pairing potential is

$$\Delta(\boldsymbol{r}_1, \boldsymbol{r}_2) = V^{pp}(\boldsymbol{r}_1, \boldsymbol{r}_2)\kappa(\boldsymbol{r}_1, \boldsymbol{r}_2), \tag{3}$$

where κ is the pairing tensor and V^{pp} is the pairing force of a density-dependent zero-range type,

$$V^{pp}(\boldsymbol{r}_1, \boldsymbol{r}_2) = V_0 \frac{1}{2}(1 - P^\sigma)\delta(\boldsymbol{r}_1 - \boldsymbol{r}_2)\left(1 - \frac{\rho(\boldsymbol{r}_1)}{\rho_{\text{sat}}}\right), \tag{4}$$

with V_0 as the pairing strength, $(1 - P^\sigma)/2$ as the projector for the spin $S = 0$ component in the pairing channel, and $\rho_{\rm sat}$ as the saturation density of nuclear matter.

For an axially deformed nucleus with spatial reflection symmetry, the potentials and densities can be expanded in terms of Legendre polynomials,

$$f(r) = \sum_\lambda f_\lambda(r) P_\lambda(\cos\theta), \quad \lambda = 0, 2, 4, \ldots, \lambda_{\max} \tag{5}$$

Finally, in DRHBc theory, the RHB equations are solved using the basis expansion method with the Dirac WS basis [25,43,44], which can properly describe the large spatial extension of weakly bound nuclei.

3. Results and Discussion

Upon the efforts of the DRHBc mass table collaboration, the mass table for even-Z nuclei in DRHBc with the PC-PK1 density functional [27] has been constructed [29–31]. The numerical details adopted here for the U, Pu, and Cm isotopic chains follow the DRHBc mass table calculations for the nuclear region $72 \leqslant Z \leqslant 100$ [28,30]. That is, the box size $R_{\rm box} = 20$ fm and the energy cutoff $E_{\rm cut} = 300$ MeV for the Dirac WS basis have been chosen. The pairing strength $V_0 = -325\ {\rm MeV} \cdot {\rm fm}^3$ and the pairing window 100 MeV are used in DRHBc theory calculations. The Legendre expansion truncation order $\lambda_{\max} = 8$ and the angular momentum cutoff $J_{\max} = 23/2\hbar$ are taken.

First of all, for these three isotopic chains, the proton and neutron drip line nuclei will be determined by the Fermi energies and the two nucleon separation energies. The Fermi energy represents the change in total energy with the change in the number of particles [45]. A negative Fermi energy usually corresponds to a positive separation energy of a bound nucleus, and a positive Fermi energy implies an unbound nucleus in the mean field level [28]. The nucleon separation energy can provide direct information on whether the nucleus is able to emit nucleons or not.

Figure 1 shows the calculated neutron Fermi energies $\lambda_{\rm n}$ and proton Fermi energy $\lambda_{\rm p}$ for the even–even U, Pu, and Cm isotopic chains in DRHBc theory calculations. For the convention where the pairing energy is zero, the Fermi energy is chosen to be the energy of the last occupied single-particle state, which is the same strategy adopted in Refs. [28,29]. In Figure 1a, it is seen that the $\lambda_{\rm n}$ almost continuously increases with the neutron number for a whole isotopic chain and finally becomes positive when going beyond the neutron drip-line. The neutron drip-line nuclei for these isotopic chains are ^{350}U, ^{352}Pu, and ^{354}Cm, respectively, all corresponding to the neutron number $N = 258$. In Figure 1b, it is seen that the $\lambda_{\rm p}$ starts from a positive value and almost continuously decreases with the proton number for a whole isotopic chain. The first nucleus with negative $\lambda_{\rm p}$ corresponds to the proton drip line, which is ^{212}U with N = 120 ($\lambda_{\rm p} = -0.16$ MeV) for U isotopes, ^{220}Pu with N = 126 ($\lambda_{\rm p} = -0.07$ MeV) for Pu isotopes, and ^{226}Cm with N = 130 ($\lambda_{\rm p} = -0.36$ MeV) for Cm isotopes. Corresponding, the three nuclei are the proton drip-line nuclei. Note that these neutron and proton drip-line nuclei determined by the Fermi energies are consistent with the results by the two-neutron separation energies $S_{2\rm n}$.

The sudden changes in the Fermi energies may suggest the possible shell closures. In Figure 1a, the $\lambda_{\rm n}$ increases rapidly at certain neutron numbers, such as the well-known magic number N = 126 in U and Pu isotopic chains and N = 184 and 258 in U, Pu, and Cm isotopic chains. The latter indicates new shell closures at N = 184 and 258. In Figure 1b, in contrast to the Pu and Cm isotopic chains, the proton Fermi energy $\lambda_{\rm p}$ in the U isotopic chain shows sudden drops when approaching the possible neutron shell closures N = 126, 184 and 258. As interpreted below, these sudden drops can be attributed to the proton pairing collapse originating from the spurious shell closure at $Z = 92$ in the single-proton energy levels.

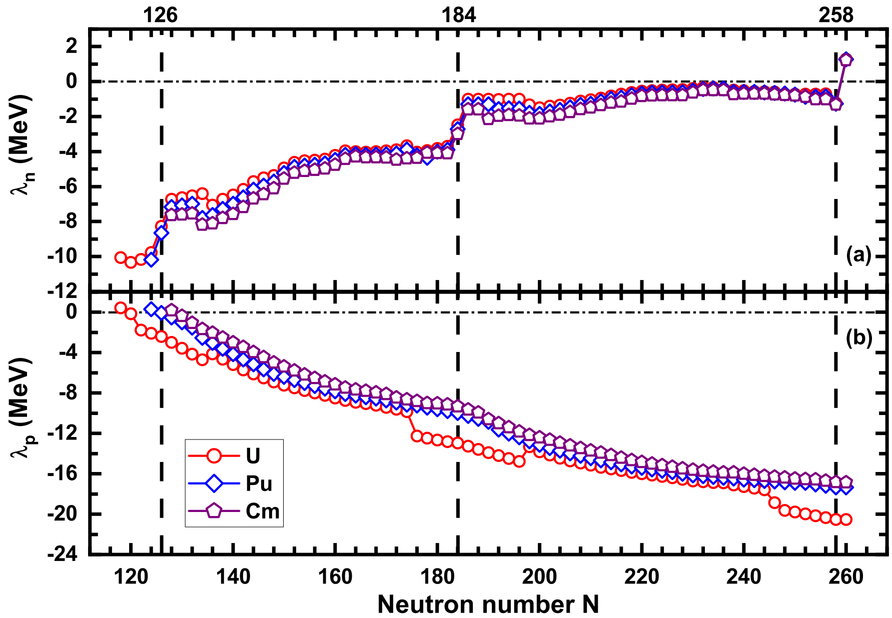

Figure 1. Neutron (**a**) and proton (**b**) Fermi energies of even−even U, Pu, and Cm isotopic chains in DRHBc theory calculations.

Taking the nuclei ^{276}U, ^{278}Pu, ^{280}Cm with $N = 184$ as an example, Figure 2 shows the single-proton levels near the Fermi energy as a function of the deformation parameter β_2. In this subfigure (a), there is a significant spherical shell gap of $Z = 92$ around 3.816 MeV between the degenerate spherical orbitals $2f_{7/2}$ and $1h_{9/2}$, which is even larger than the traditional spherical shell of $Z = 82$, as shown below. Due to the existence of this proton shell $Z = 92$, the U isotopes with neutron number not far away from shell closures tend to be spherical, and the corresponding proton pairing energy tends to be zero. This pairing collapse leads the proton Fermi energies around N = 184 for these Uranium isotopes located at the designated spherical orbital $1h_{9/2}$. For the neighboring uranium isotopes away from N = 184, the ground states are deformed with Fermi energies above $1h_{9/2}$. As a result, in Figure 1b, focusing the neutron numbers around the possible shell closure N = 184, there is one sudden drop from 174 to 176, jumping from Fermi energies above $1h_{9/2}$ in deformed nuclei to exactly $1h_{9/2}$ when pairing collapse occurs, together with one sudden rise from 196 to 198 when shape transition from spherical to deformed occurs. The shape evolution will be further discussed with quadrupole deformation later. For Pu and Cm isotopes with two or four more protons, in Figure 2b,c, the Fermi energies just stay between these two orbitals $1h_{9/2}$ and $2f_{7/2}$, both for spherical ground states close to N = 184 and for deformed ground states away from 184. Consequently, the Fermi energies around N = 184 for Pu and Cm isotopes displayed continuous behavior without abrupt changes as shown in Figure 1b. This spurious shell closure $Z = 92$, which is commonly found in the CDFT calculations, is expected to be cured or mitigated by the presence of tensor interaction [46] or localized Fock term [47].

From the binding energies, the two-neutron separation energies S_{2n} can be calculated as

$$S_{2n}(Z, N) = E_B(Z, N) - E_B(Z, N-2). \tag{6}$$

In Figure 3a, the S_{2n} values in the U, Pu, and Cm isotopic chains obtained from the DRHBc calculations are shown, in comparison with the RCHB results [48] and the available experimental data [38]. Around the shell closure $N = 126$, the results of the DRHBc and the

RCHB are consistent and reproduce its robustness in the vicinity of proton drip line [41]. Away from the shell-closure region, compared to the RCHB results, the DRHBc calculations reproduce the experimental values better. When the S_{2n} reaches a negative value, the nucleus is unbound against two-neutron emission. The last nucleus with the positive S_{2n} is determined as the two-neutron drip line nucleus. In the even–even U, Pu, and Cm isotopic chains, the last positive values are 1.41 MeV of ^{350}U, 1.73 MeV of ^{352}Pu, and 2.00 MeV of ^{354}Cm; thus, these three nuclei are at the two-neutron drip line $N = 258$. This is consistent with the position of the neutron drip line determined by the λ_n in Figure 1a.

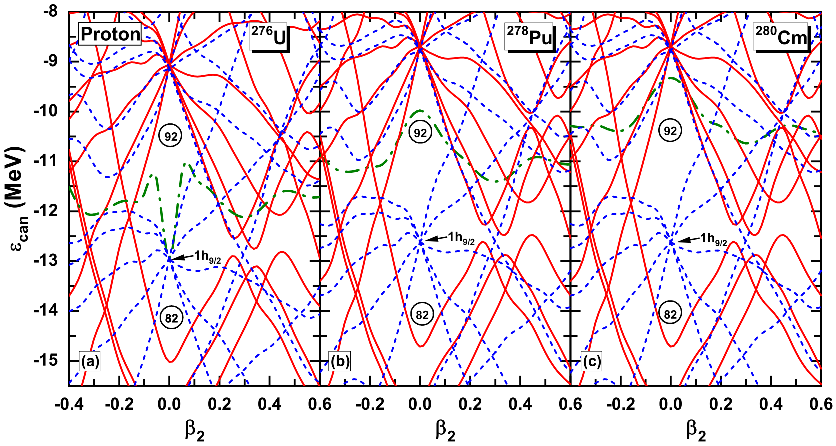

Figure 2. Single−proton energies in the canonical basis of ^{276}U (**a**), ^{278}Pu (**b**) , ^{280}Cm (**c**) as a function of the deformation parameter β_2 in DRHBc theory calculations. The Fermi energy as a function of quadrupole deformation is also displayed by a green dash−dot line. The single-particle levels with positive (negative) parity are displayed as red solid (blue dashed) lines. The proton number obtained by filling all the lower levels is shown with a circle at several energy gaps.

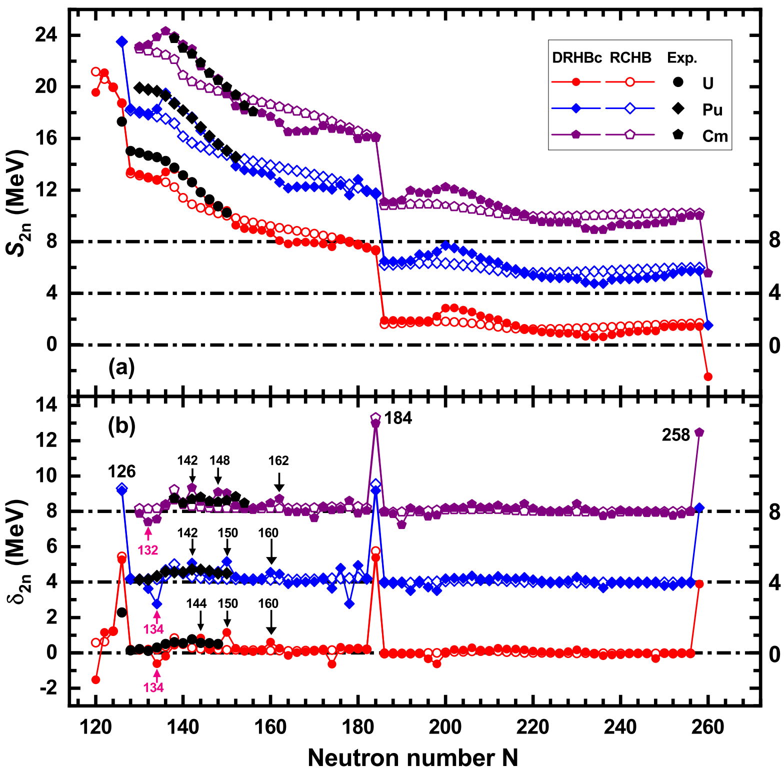

Figure 3. Two−neutron separation energies (**a**) and two−neutron shell gaps (**b**) of even−even U, Pu (shifted up 4 MeV), and Cm (shifted up 8 MeV) isotopic chains in DRHBc theory calculations. The RCHB results [48] and the available experimental data [38] are shown for comparison.

In Figure 3a, between the traditional shell closure $N = 126$ and two possible ones $N = 184$ and 258, comparing with the RCHB results, the S_{2n} from DRHBc theory exhibits systematic behavior. When the neutron number increases from the shell closure to the middle shell, S_{2n} from DRHBc theory is higher than that of RCHB calculation, while from the mid-shell to the next shell closure, S_{2n} from DRHBc theory is lower than that of RCHB calculation. It is noteworthy that the RCHB theory is spherical, while DRHBc theory takes the quadrupole deformation into account. Such behavior should be associated with the evolution of the ground state deformation.

It is further noted that some bound nuclei beyond the neutron drip line have been predicted in the DRHBc mass table calculations [30,31], such as in the $50 \leqslant Z \leqslant 70$ [35] and $106 \leqslant Z \leqslant 112$ [33,49,50] regions, which form the peninsulas of stability in the nuclear landscape. However, for the current region, after examining the neutron Fermi energies and the two-neutron separation energies for nuclei beyond the neutron drip line, this phenomenon of entrant stability is not found.

Besides the information of drip line, the S_{2n} contains detailed information about the shell closure. For example, as shown in Figure 3a, the S_{2n} in the U, Pu, and Cm isotopic chains show sudden drops at the traditional magic number $N = 126$ and possible magic numbers $N = 184$ and 258. Away from the shell closures, as the number of neutrons increases, the S_{2n} drops almost smoothly. However, near $N = 134$ and $N = 198$, the S_{2n} calculated using DRHBc theory shows a slight increase with the neutron number, whereas the S_{2n} obtained from RCHB theory does not exhibit the increasing behavior. Similar increases of S_{2n} are also observed in the DRHBc results at positions such as near $N = 174$, 248 in the U isotopic chain; $N = 174$, 178, 192, 236 in the Pu isotopic chain; and $N = 170$, 190 in the Cm isotopic chain. It is noteworthy that RCHB theory is spherical, while DRHBc theory takes the quadrupole deformation into account. Thus the quadrupole deformation may lead to the occurrence of these phenomena.

In order to more clearly demonstrate the shell closures and the fine structure of S_{2n} in the U, Pu, and Cm isotopic chains, the two-neutron shell gaps δ_{2n}, which are the difference of S_{2n} between two neighboring nuclei

$$\delta_{2n}(Z, N) = S_{2n}(Z, N) - S_{2n}(Z, N+2), \tag{7}$$

are analyzed. Figure 3b shows the δ_{2n} of the even–even U, Pu, and Cm isotopic chains calculated by DRHBc theory with the neutron number together with the RCHB results [48] and the available experimental data [38]. Comparing with the RCHB results, DRHBc theory better reproduces the available experimental data. At the shell closures or possible shell closures $N = 126$, 184 and 258, the δ_{2n} obtained from both the DRHBc and RCHB calculations always exhibits pronounced peaks in the U, Pu, and Cm isotopic chains. As shown in Figure 3b, most δ_{2n} values, whether from the RCHB calculations or the DRHBc calculations, are non-negative, reflecting the globally declining behavior of S_{2n} with the increase in neutron number. The few negative δ_{2n} values appear only in the DRHBc results, the positions of which are around $N = 134$ and 198 for the three isotopic chains and also at $N = 174$, 248 for U, $N = 174$, 178, 192, 236 for Pu, and $N = 170$, 190 for Cm. In comparison, the δ_{2n} is always greater than zero for the RCHB results, which does not consider the quadrupole deformation degree of freedom. Therefore, it is necessary to examine the quadrupole deformation evolutions in these isotopic chains.

Figure 4 presents the ground state deformation evolutions of the U, Pu, and Cm isotopic chains obtained from the DRHBc calculations, in comparison with the available empirical data extracted from the observed $B(\mathrm{E2}, 0_1^+ \to 2_1^+)$ [38]. DRHBc theory can reproduce the available data. As seen in Figure 4, the deformation evolutions of the even–even U, Pu, and Cm isotopic chains show similar evolutionary patterns: near the well-known shell closure at $N = 126$, the ground state shapes are spherical or nearly spherical. Before reaching the next shell closure at $N = 184$, β_2 reaches a peak in the mid-shell. As the neutron number increases to $N = 172$, ^{268}Cm is the first to transit from prolate to oblate shape, followed by ^{268}Pu at $N = 174$ and ^{268}U at $N = 176$. From $N = 184$ to possible shell closure at $N = 258$, they all first experience a transition from spherical to prolate, with β_2 reaching a peak around $N = 214$. The U, Pu, and Cm isotopic chains experience transitions from prolate to oblate shape at $N = 236$, $N = 238$, and $N = 238$, respectively. After that, the ground state shape becomes less oblate with increasing neutron number, and finally becomes spherical at $N = 258$.

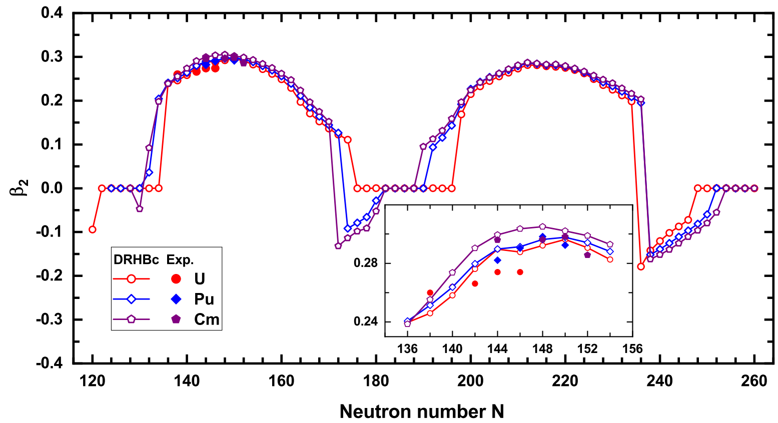

Figure 4. Quadrupole deformation of even−even U, Pu, and Cm isotopic chains in DRHBc theory calculations, and the available experimental data [38] are shown for comparison. The inset gives a detailed comparison between the calculated results and the available experimental data [38].

One may notice that the increase in S_{2n} in Figure 3a and the negative δ_{2n} in Figure 3b appear where the quadrupole deformation transition happens in Figure 4. For example, the negative δ_{2n} occurs at N = 134 for U and Pu isotopes, and N = 132 for Cm isotopes; correspondingly the shape transition from spherical to prolate occurs synchronically in Figure 4.

Besides the pronounced peaks of δ_{2n} that show the major shells at $N = 126$, 184, and 258, in Figure 3b, one can also find some small-scale peaks in the DRHBc results. The amplitudes of these peaks are about 1 MeV or less, and their positions are not strictly aligned for different isotopic chains. For uranium, these small peaks appear at N = 144, 150, and 160; for plutonium, at N = 142, 150, and 160; and for curium, at N = 142, 148, and 162. Note that these peaks do not appear in the RCHB results, but instead another small peak at $N = 138$ appears.

To understand the origins of these small peaks in Figure 3b, by comparing the U, Pu, and Cm isotones, Figure 5 shows the canonical single-neutron energies of ^{234,242,252}U, ^{236,244,254}Pu and ^{238,246,256}Cm as a function of the deformation parameter β_2 obtained by DRHBc theory. When the nucleus is spherical at $\beta_2 = 0$, the neutron single particle levels with the same quantum numbers nlj are degenerate due to the spherical symmetry, leading to several energy gaps between two neighboring spherical orbitals. The energy gap between the spherical orbitals $1i_{11/2}$ and $2g_{9/2}$ is around 2 MeV. With the $1i_{11/2}$ orbital fully occupied by 12 neutrons lying above the shell closure N = 126, a spherical gap at N = 138 is formed. This can be used to interpret the small peak of δ_{2n} at N = 138 shown by the spherical RCHB results in Figure 3.

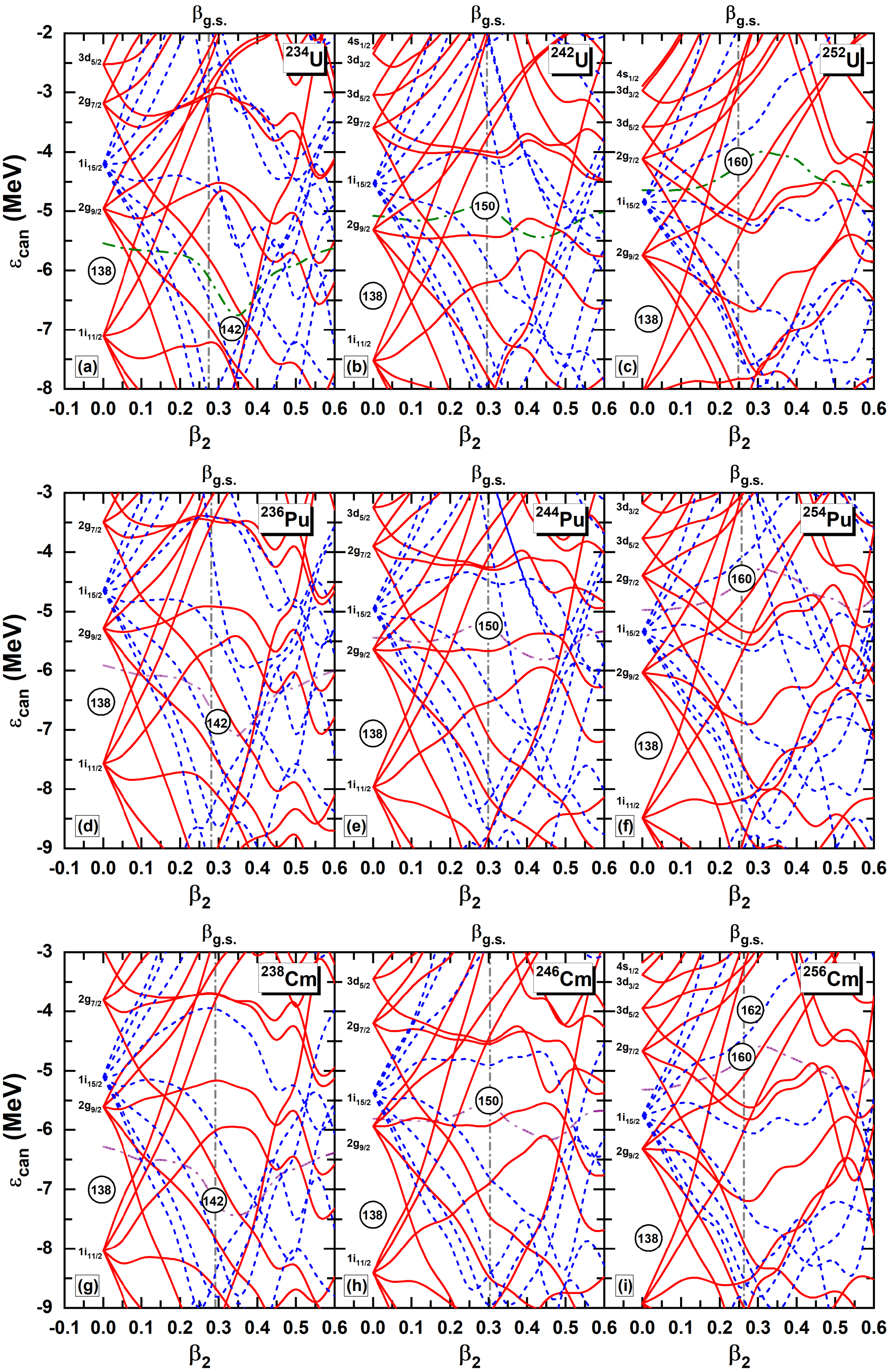

Figure 5. Single−neutron energies in the canonical basis for uranium, plutonium and curium isotopes with N = 142, 150 and 160, namely ^{234,242,252}U (**a**−**c**), ^{236,244,254}Pu (**d**−**f**), and ^{238,246,256}Cm (**g**−**i**), as functions of the deformation parameter β_2 in DRHBc theory. The Fermi energy is also displayed by a green dash−dot line. The single−particle levels with positive (negative) parity are displayed as red solid (blue dashed) lines. The neutron numbers obtained by filling all the lower levels are shown in a circle at several energy gaps. The ground states are indicated by gray lines at corresponding deformation positions.

When the spherical symmetry is broken and a nucleus undergoes axial deformation, the total angular momentum j is no longer a good quantum number while its projection on the symmetry axis K remains a good quantum number. Normally, one spherical j-shell splits into $(2j+1)/2$ orbitals. As a result, the traditional spherical shell closure breaks down and new deformed subshells may emerge. As shown in Figure 5, comparing panels (a), (d), and (g), a shell gap at 142 appears obviously for the $N = 142$ isotones ^{236}Pu and ^{238}Cm but not so distinctly for $N = 142$ isotone ^{234}U. Instead, for ^{234}U, a gap slightly larger appears at $N = 144$, just above 142. This gap change effectively explains the subtle peak shift from $N = 144$ for U to $N = 142$ for Cm in Figure 3b. Similarly, a gap at 160 emerges for $N = 160$ isotones ^{252}U and ^{254}Pu in panel (c) and (f), while a gap at 162 is seen for ^{256}Cm in panel (i), corresponding to the peak shift from $N = 160$ for U and Pu to $N = 162$ for Cm in Figure 3b. For panels (b) ,(e), and (h), a relatively robust subshell gap at $N = 150$ can be found for ^{242}U, ^{244}Pu, and ^{246}Cm, which generally agrees with the peak at $N = 150$ for U, Pu in Figure 3b. Based on the analysis, the small peak of two neutron gap δ_{2n} strongly correlates with the deformed subshell structure near the Fermi surface, and some subshells may be quenched with different isotopic chains.

Another important indicator of shell closure is the average pairing gap, as discussed in Ref. [51], which allows us to obtain direct information about the impact of pairing correlations and shows the arch structures that vanish at shell closures and have additional deeps at subshell closures. Figure 6a shows the Δ_n as a function of the number of neutrons for even–even U, Pu, and Cm isotopic chains calculated by DRHBc theory. As shown in Figure 6a, most Δ_n values transition smoothly with the neutron number and are greater than zero. However, near the magic number N = 126 and the possible magic numbers N = 184 and 258, Δ_n values exhibit a sharp decrease and become zero. Additionally, we observe that a few Δ_n values also show a decrease at the following positions: for the U isotopic chain, N = 144, 150, and 160; for the Pu isotopic chain, N = 142, 150, and 160; and for the Cm isotopic chain, N = 142, 148, and 162. These positions correspond to the small-scale peaks in Figure 3b.

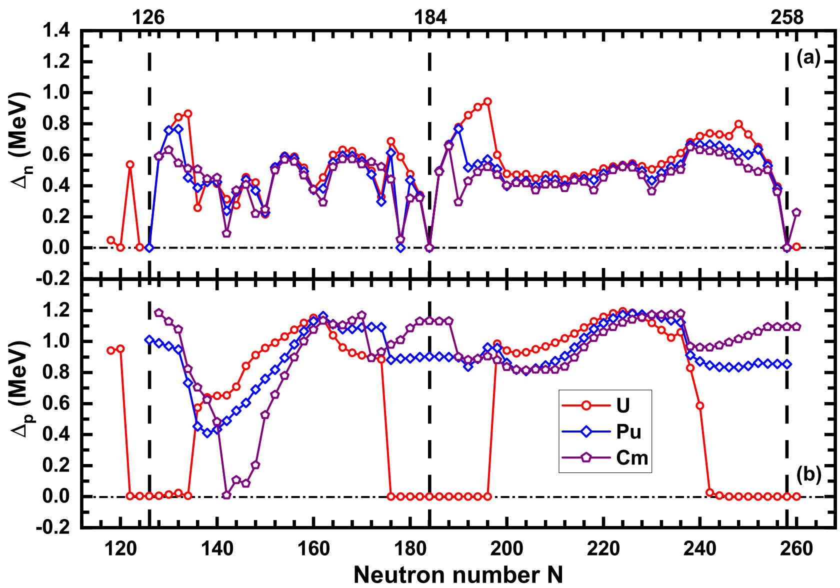

Figure 6. Neutron average pairing gap Δ_n (**a**) and proton average pairing gap Δ_p (**b**) of even−even U, Pu, and Cm isotopic chains in DRHBc theory calculations.

Figure 6b shows the Δ_p as a function of the number of protons for even–even U, Pu, and Cm isotopic chains calculated by DRHBc theory. Similarly, in Figure 6b, most Δ_p values exceed zero. It is observed that for the U isotopic chain, Δ_p values drop to zero near the magic number $N = 126$ and the possible magic numbers $N = 184$ and 258. In contrast, the Δ_p values for Pu and Cm isotopic chains remain positive. This indicates that due to the existence of the pseudo shell $Z = 92$, a pairing collapse occurs in the U isotopic chain within these regions, resulting in a sudden decrease in the λ_p value in the U isotopic chain shown in Figure 1.

Very recently, Ref. [52] proposed a new binding-energy indicator, single-particle neutron energy Δe_n , to catalog the subshell closures in nuclear landscape. This indicator behaves in a similar way as $\delta_{2\mathrm{n}}$. The subshell closures at $N = 152$ and 162 are found for different mass models SkM*, SLy4, UNEDF1, UNEDF2, and FRDM-2012. These two subshells are very close to our results presented here.

4. Conclusions

In summary, we have performed systematic studies of DRHBc theory with the PC-PK1 density functional for the shell structure evolution of even–even U, Pu, and Cm isotopic chains from the proton drip line to the neutron drip line. By analyzing the Fermi energies and the two-neutron separation energies, we predicted the proton drip line for the U, Pu, and Cm isotopic chains to be at ^{212}U, ^{220}Pu, and ^{226}Cm and the neutron drip line to be at ^{350}U, ^{352}Pu, and ^{354}Cm, respectively. In comparison with spherical RCHB calculations, the inclusion of axial deformation degree of freedom does not change these drip line boundaries. The phenomenon of entrant stability beyond the neutron drip line is not found for the current region. The shell closures at $N = 126$, 184, and 258 in U, Pu, and Cm isotopic chains can be clearly seen by the Fermi energy λ_n, two-neutron separation energy $S_{2\mathrm{n}}$, and two-neutron shell gap $\delta_{2\mathrm{n}}$. The emergence of sudden drops between U and Pu isotopic chains in the proton Fermi energies λ_p around some neutron shell closures $N = 126$, 184, and 258 is a consequence of designation convention when the pairing collapse at the spurious shell closure $Z = 92$ occurs.

The fine structure in the two-neutron separation energy and the two-neutron shell gap, like decrease of $S_{2\mathrm{n}}$ and negative $\delta_{2\mathrm{n}}$, may be related to the ground state shape transition.

Finally, the small-scale peaks in the two-neutron shell gaps $\delta_{2\mathrm{n}}$ indicate some subshells, namely, $N = 144$, 150, and 160 for uranium, $N = 142$, 150, and 160 for plutonium, and $N = 142$, 148, and 162 for curium. These subshells can be well understood by the deformed gaps in the single-neutron levels obtained by DRHBc theory.

Author Contributions: Conceptualization, W.Z. and J.P.; methodology, L.W.; software, J.H.; formal analysis, L.W.; investigation, L.W.; resources, W.Z.; data curation, J.H.; writing—original draft preparation, L.W.; writing—review and editing, J.P.; visualization, L.W.; supervision, W.Z. All authors have read and agreed to the published version of the manuscript.

Funding: This work was partly supported by the Natural Science Foundation of Henan Province (Grant No. 242300421156, 202300410480), the National Natural Science Foundation of China (Grant No. U2032141), and the Super Computing Center of Beijing Normal University.

Data Availability Statement: The study does not report any finalized data yet.

Acknowledgments: All authors deeply thank Shuang-quan Zhangfor detailed discussion and revision. Helpful discussions with members of the DRHBc Mass Table Collaboration are highly appreciated.

Conflicts of Interest: The authors declare no conflicts of interest.

References

1. Sorlin, O.; Porquet, M.-G. Nuclear magic numbers: New features far from stability. *Prog. Part. Nucl. Phys.* **2008**, *61*, 602.
2. Otsuka, T.; Gade, A.; Sorlin, O.; Suzuki, T.; Utsuno, Y. Evolution of shell structure in exotic nuclei. *Rev. Mod. Phys.* **2020**, *92*, 015002.

3. Zhan, W.L.; Xu, H.S.; Xia, J.W.; Zhao, H.W.; Yuan, Y.J. Progress in HIRFL-CSR. *Nucl. Phys. A* **2010**, *834*, 694c.
4. Motobayashi, T. RIKEN RI Beam Factory-Recent Results and Perspectives. *Nucl. Phys. A* **2010**, *834*, 707c.
5. Thoennessen, M. Plans for the Facility for Rare Isotope Beams. *Nucl. Phys. A* **2010**, *834*, 688c.
6. Dinca, D.C.; Janssens, R.V.F.; Gade, A.; Bazin, D.; Broda, R.; Brown, B.A.; Campbell, C.M.; Carpenter, M.P.; Chowdhury, P.; Cook, J.M.; et al. Reduced transition probabilities to the first 2+ state in Ti-52,54,56 and development of shell closures at N=32,34. *Phys. Rev. C* **2005**, *71*, 041302.
7. Steppenbeck, D.; Takeuchi, S.; Aoi, N.; Doornenbal, P.; Matsushita, M.; Wang, H.; Baba, H.; Fukuda, N.; Go, S.; Honma, M.; et al. Evidence for a new nuclear 'magic number' from the level structure of ^{54}Ca. *Nature* **2013**, *502*, 207.
8. de Groote, R.P.; Billowes, J.; Binnersley, C.L.; Bissell, M.L.; Cocolios, T.E.; Day Goodacre, T.; Farooq-Smith, G.J.; Fedorov, D.V.; Flanagan, K.T.; Franchoo, S.; et al. Measurement and microscopic description of odd–even staggering of charge radii of exotic copper isotopes. *Nat. Phys.* **2020**, *16*, 620.
9. Bender, M.; Heenen P.H.. Self-consistent mean-field models for nuclear structure. *Rev. Mod. Phys.* **2003**, *75*, 121.
10. Meng, J.; Toki, H.; Zhou, S.G.; Zhang, S.Q.; Long, W.H.; Geng, L.S. Relativistic Continuum Hartree Bogoliubov theory for ground state properties of exotic nuclei. *Prog. Part. Nucl. Phys.* **2006**, *57*, 470.
11. Samyn, M.; Goriely, S.; Heenen, P.-H.; Pearson, J.M.; Tondeur, F. A Hartree–Fock–Bogoliubov mass formula. *Nucl. Phys. A* **2002**, *700*, 142.
12. Stoitsov, M.V.; Dobaczewski, J.; Nazarewicz, W.; Pittel, S.; Dean, D.J. Systematic study of deformed nuclei at the drip lines and beyond. *Phys. Rev. C* **2003**, *68*, 054312.
13. Goriely, S.; Chamel, N.; Pearson, J.M. Skyrme-Hartree–Fock–Bogoliubov nuclear mass formulas: Crossing the 0.6 MeV threshold with microscopically deduced pairing. *Phys. Rev. Lett.* **2009**, *102*, 152503.
14. Goriely, S.; Chamel, N.; Pearson, J.M. Further explorations of Skyrme-Hartree–Fock–Bogoliubov mass formulas. 13. The 2012 atomic mass evaluation and the symmetry coefficient. *Phys. Rev. C* **2013**, *88*, 024308.
15. Hilaire, S.; Girod, M. Large-scale mean-field calculations from proton to neutron drip lines using the D1S Gogny force. *Eur. Phys. J. A* **2007**, *33*, 237.
16. Goriely, S.; Hilaire, S.; Girod, M. First Gogny-Hartree–Fock–Bogoliubov Nuclear Mass Model. *Phys. Rev. Lett.* **2009**, *102*, 242501.
17. Delaroche, J.P.; Girod, M.; Libert, J.; Goutte, H.; Hilaire, S.; Peru, S.; Pillet, N.; Bertsch, G.F. Structure of even–even nuclei using a mapped collective Hamiltonian and the D1S Gogny interaction. *Phys. Rev. C* **2010**, *81*, 014303.
18. Ring, P. Relativistic mean field in finite nuclei. *Prog. Part. Nucl. Phys.* **1996**, *37*, 193.
19. Vretenar, D.; Afanasjev, A.V.; Lalazissis, G.A.; Ring, P. Relativistic Hartree Bogoliubov theory: static and dynamic aspects of exotic nuclear structure. *Phys. Rep.* **2005**, *409*, 101.
20. Niksic, T.; Vretenar, D.; Ring, P. Relativistic Nuclear Energy Density Functionals: Mean-Field and Beyond. *Prog. Part. Nucl. Phys.* **2011**, *66*, 519.
21. Meng, J.; Peng, J.; Zhang, S.Q.; Zhao, P.W. Progress on tilted axis cranking covariant density functional theory for nuclear magnetic and antimagnetic rotation. *Front. Phys.* **2013**, *8*, 55.
22. Meng, J.; Zhou, S.G. Halos in medium-heavy and heavy nuclei with covariant density functional theory in continuum. *J. Phys. G* **2015**, *42*, 093101.
23. Zhou, S.G. Multidimensionally constrained covariant density functional theories-nuclear shapes and potential energy surfaces. *Phys. Scr.* **2016**, *91*, 063008.
24. Shen, S.H.; Liang, H.Z.; Long, W.H.; Meng, J.; Ring, P. Towards an *abinitio* covariant density functional theory for nuclear structure. *Prog. Part. Nucl. Phys.* **2019**, *109*, 103713.
25. Zhou, S.G.; Meng, J.; Ring, P.; Zhao, E.G. Neutron halo in deformed nuclei. *Phys. Rev. C* **2010**, *82*, 011301.
26. Li, L.L.; Meng, J.; Ring, P.; Zhao, E.G.; Zhou, S.G. Deformed relativistic Hartree Bogoliubov theory in continuum. *Phys. Rev. C* **2012**, *85*, 024312.
27. Zhao, P.W.; Li, Z.P.; Yao, J.M.; Meng, J. New parametrization for the nuclear covariant energy density functional with a point-coupling interaction. *Phys. Rev. C* **2010**, *82*, 054319.
28. Zhang, K.Y.; Cheoun, M.K.; Choi, Y.B.; Chong, P.S.; Dong, J.M.; Geng, L.S.; Ha, E.; He, X.T.; Heo, C.; Ho, M.C.; et al. Deformed relativistic Hartree–Bogoliubov theory in continuum with a point-coupling functional: Examples of even–even Nd isotopes. *Phys. Rev. C* **2020**, *102*, 024314.
29. Pan, C.; Cheoun, M.K.; Choi, Y.B.; Dong, J.M.; Du, X.K.; Fan, X.H.; Gao, W.; Geng, L.S.; Ha, E.; He, X.T.; et al. Deformed relativistic Hartree–Bogoliubov theory in continuum with a point-coupling functional. II. Examples of odd Nd isotopes. *Phys. Rev. C* **2022**, *106*, 014316.
30. Zhang, K.Y.; Cheoun, M.K.; Choi, Y.B.; Chong, P.S.; Dong, J.M.; Dong, Z.H.; Du, X.K.; Geng, L.S.; Ha, E.; He, X.T.; et al. Nuclear mass table in deformed relativistic Hartree–Bogoliubov theory in continuum, I: Even–even nuclei. *At. Data Nucl. Data Tables* **2022**, *144*, 101488.

31. Guo, P.; Cao, K.; Chen, K.; Chen, Z.; Cheoun, M. K.; Choi, Y.B.; Lam, P.C.; Deng, W.; Dong, J.; Du, X.; et al. Nuclear mass table in deformed relativistic Hartree–Bogoliubov theory in continuum, II: Even-Z nuclei. *At. Data Nucl. Data Tables* **2024**, *158*, 101661.
32. Sun, X.X.; Zhao, J.; Zhou, S.G. Study of ground state properties of carbon isotopes with deformed relativistic Hartree–Bogoliubov theory in continuum. *Nucl. Phys. A* **2020**, *1003*, 122011.
33. He, X.T.; Wang, C.; Zhang, K.Y.; Shen, C.W. Possible existence of bound nuclei beyond neutron drip lines driven by deformation. *Chin. Phys. C* **2021**, *45*, 101001.
34. In, E.J.; Kim, Y.; Papakonstantinou, P.; Hong, S.W. Neutron drip line in the deformed relativistic Hartree–Bogoliubov theory in continuum: Oxygen to Calcium. *Int. J. Mod. Phys. E* **2021**, *30*, 2150009.
35. Pan, C.; Zhang, K.Y.; Chong, P.S.; Heo, C.; Ho, M.C.; Lee, J.; Li, Z.P.; Sun, W.; Tam, C.K.; Wong, S.H.; et al. Possible bound nuclei beyond the two-neutron drip line in the $50 \leq Z \leq 70$ region. *Phys. Rev. C* **2021**, *104*, 024331.
36. Mun, M.H.; Kim, S.; Cheoun, M.K.; So, W.Y.; Choi, S.; Ha, E. odd–even shape staggering and kink structure of charge radii of Hg isotopes by the deformed relativistic Hartree–Bogoliubov theory in continuum. *Phys. Lett. B* **2023**, *847*, 138298.
37. Guo, P.; Pan, C.; Zhao, Y.C.; Du, X.K.; Zhang, S.Q. Prolate-shape dominance in atomic nuclei within the deformed relativistic Hartree–Bogoliubov theory in continuum. *Phys. Rev. C* **2023**, *108*, 014319.
38. Wang, M.; Huang, W.J.; Kondev, F.G.; Audi, G.; Naimi, S. The AME 2020 atomic mass evaluation (II). Tables, graphs and references. *Chin. Phys. C* **2021**, *45*, 030003.
39. Zheng, R.Y.; Sun, X.X.; Shen, G.F.; Geng, L.S. Evolution of N = 20, 28, 50 shell closures in the $20 \leq Z \leq 30$ region in deformed relativistic Hartree–Bogoliubov theory in continuum. *Chin. Phys. C* **2024**, *48*, 014107.
40. Zhang, W.; Huang, J.K.; Sun, T.T.; Peng, J.; Zhang, S.Q. Inner fission barriers of uranium isotopes in the deformed relativistic Hartree–Bogoliubov theory in continuum. *Chin. Phys. C* **2024**, *48*, 104105.
41. Zhang, Z.Y.; Gan, Z.G.; Yang, H.B.; Ma, L.; Huang, M.H.; Yang, C.L.; Zhang, M.M.; Tian, Y.L.; Wang, Y.S.; Sun, M.D.; et al. New Isotope Np220 : Probing the Robustness of the N=126 Shell Closure in Neptunium. *Phys. Rev. Lett.* **2019**, *122*, 192503.
42. Li, L.L.; Meng, J.; Ring, P.; Zhao, E.G.; Zhou, S.G. Odd systems in deformed relativistic Hartree Bogoliubov theory in continuum. *Chin. Phys. Lett.* **2012**, *29*, 042101.
43. Zhang, K.Y.; Pan, C.; Zhang, S.Q. Optimized Dirac Woods-Saxon basis for covariant density functional theory. *Phys. Rev. C* **2022**, *106*, 024302.
44. Zhou, S.G.; Meng, J.; Ring, P. Spherical relativistic Hartree theory in a Woods-Saxon basis. *Phys. Rev. C* **2003**, *68*, 034323.
45. Ring, P.; Schuck, P. *The Nuclear Many-Body Problem*; Springer: Berlin/Heidelberg, Germany, 1980.
46. Liang, H.Z.; Meng, J.; Zhou, S.G. Hidden pseudospin and spin symmetries and their origins inatomic nuclei. *Phys. Rep.* **2015**, *570*, 1.
47. Zhao, Q.; Ren, Z.X.; Zhao, P.W.; Meng, J. Covariant density functional theory with localized exchange terms. *Phys. Rev. C* **2022**, *106*, 034315.
48. Xia, X.W.; Lim, Y.; Zhao, P.W.; Liang, H.Z.; Qu, X.Q.; Chen, Y.; Liu, H.; Zhang, L.F.; Zhang, S.Q.; Kim, Y.; et al. The limits of the nuclear landscape explored by the relativistic continuum Hartree–Bogoliubov theory. *At. Data Nucl. Data Tables* **2018**, *121*, 1.
49. Zhang, K.Y.; He, X.T.; Meng, J.; Pan, C.; Shen, C.W.; Wang, C.; Zhang, S.Q. Predictive power for superheavy nuclear mass and possible stability beyond the neutron drip line in deformed relativistic Hartree–Bogoliubov theory in continuum. *Phys. Rev. C* **2021**, *104*, L021301.
50. He, X.T.; Wu, J.W.; Zhang, K.Y.; Shen, C.W. odd–even differences in the stability peninsula in the $106 \leq Z \leq 112$ region with the deformed relativistic Hartree–Bogoliubov theory in continuum. *Phys. Rev. C* **2024**, *110*, 014301.
51. Sil, T.; Patra, S.K.; Sharma, B.K.; Centelles, M.; Viñas, X. Superheavy nuclei in a relativistic effective Lagrangian model. *Phys. Rev. C* **2004**, *69*, 044315.
52. Buskirk, L.; Godbey, K.; Nazarewicz, W.; Satula, W. Nucleonic shells and nuclear masses. *Phys. Rev. C* **2024**, *109*, 044311.